

Dynamic Dosing Assay Relating Real-Time Respiration Responses of *Staphylococcus aureus* Biofilms to Changing Microchemical Conditions

Jinzi Deng,[†] Adit Dhummakupt,[‡] Philip C. Samson,[§] John P. Wikswa,^{§,||} and Leslie M. Shor*^{†,‡,⊥}

[†]Department of Chemical & Biomolecular Engineering, University of Connecticut, Storrs, Connecticut 06269, United States

[‡]Department of Molecular Genetics & Microbiology, University of Florida College of Medicine, Gainesville, Florida, United States

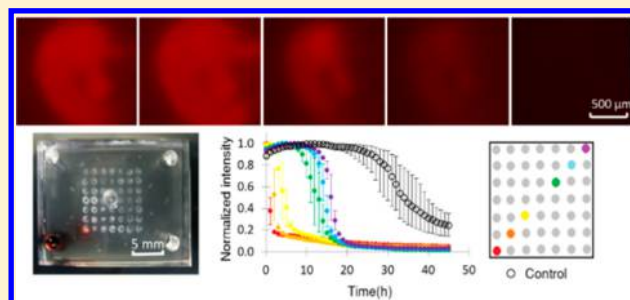
[§]Vanderbilt Institute for Integrative Biosystems Research and Education (VIIBRE), Vanderbilt University, Nashville, Tennessee 37235, United States

^{||}Departments of Biomedical Engineering, Physics & Astronomy, and Molecular Physiology & Biophysics, Vanderbilt University, Nashville, Tennessee 37235, United States

[⊥]Center for Environmental Sciences and Engineering, University of Connecticut, Storrs, Connecticut 06269, United States

Supporting Information

ABSTRACT: Bacterial biofilms are a metabolically heterogeneous community of bacteria distributed in an extracellular matrix comprised primarily of hydrated polysaccharides. Effective inhibitory concentrations measured under planktonic conditions are not applicable to biofilms, and inhibition concentrations measured for biofilms vary widely. Here, we introduce a novel microfluidic approach for screening respiration inhibition of bacteria in a biofilm array morphology. The device geometry and operating conditions allow antimicrobial concentration and flux to vary systematically and predictably with space and time. One experiment can screen biofilm respiratory responses to many different antimicrobial concentrations and dosing rates in parallel. To validate the assay, onset of respiration inhibition following NaN_3 exposure is determined optically using an O_2 -sensing thin film. Onset of respiration inhibition obeys a clear and reproducible pattern based on time for diffusive transport of the respiration inhibitor to each biofilm in the array. This approach can be used for high-throughput screening of antimicrobial effectiveness as a function of microbial characteristics, antimicrobial properties, or antimicrobial dosing rates. The approach may also be useful in better understanding acquired antimicrobial resistance or for screening antimicrobial combinations.



Bacterial biofilms are comprised of pure or mixed cultures distributed in a self-secreted hydrogel matrix. Respiration of living cells within the biofilm and the absence of bulk mixing cause microscale gradients to persist in biofilms, as typified by decreasing O_2 concentrations with depth for aerobic biofilms.¹ Persistent gradients promote phenotypic differentiation, while proximity of cells facilitates lateral transfer of antimicrobial resistance genes.² In addition to their importance in clinical settings, biofilms in industry reduce the efficiency of water desalination³ and heat exchangers.⁴ In environmental systems, biofilms can protect bacteria from predation,⁵ they protect plant roots from pathogens,⁶ and they help retain moisture in soils.⁷

Biofilm-associated bacteria exist in a distinct physiological state from planktonic cells, so inhibitory concentrations measured for planktonic cultures do not apply to biofilms. Generally speaking, biofilm-associated bacteria can tolerate much higher antimicrobial concentrations than can planktonic cultures.^{8,9} For example, Anderl et al. show that bacteria growing as a “biofilm” on an agar plate exhibit a markedly different antimicrobial susceptibility than bacteria grown in liquid suspension. In their work,

antimicrobial exposures that reduced the number of live planktonic cells by 4 orders of magnitude caused virtually no change in the biofilm-associated cultures.¹⁰

Further complicating matters, antimicrobial susceptibility of biofilms varies widely,^{11,12} due to differences between parent and mutant strains¹³ or among phenotypes¹⁴ or due to adaptation to experimental conditions.¹⁵ For example, Nelson et al. reported that minimum biofilm eradication concentrations (MBEC_{99,9}) for *Pseudomonas aeruginosa* PA14 biofilms differ by a factor of 24.¹⁴

The methods used to study biofilm inhibition by antimicrobials include flow cells, diffusion cells, multiwell plates, chemostats, and microfluidic devices. These techniques can usually be classified as high-throughput or high-content. High-throughput screening of biofilm antimicrobial susceptibility is

Received: December 29, 2012

Accepted: April 30, 2013

Published: April 30, 2013

most often done using well plates^{16–18} or their variations where biofilms are cultured on coupons,¹⁹ on lid pegs,²⁰ or in microfluidic channels between wells.²¹ Well-plate methods are widely used to measure the minimum inhibitory concentration (MIC) and other aspects of antimicrobial environments.¹⁷ However, the inferior optical properties of many high-throughput platforms lead to a reliance on disruptive staining assays and measurement of aggregate responses at a single time point.

In contrast to one-time observations in most high-throughput assays, high-content techniques frequently feature real-time observation of cellular responses by tracking a fluorescent tag²² or variation in optical density.²³ Some biofilm studies are carried out in flow cells that allow visualization of attachment and biofilm development as a function of shear stress^{24–26} or changing chemical conditions.²⁷ Other flow cell studies have monitored biofilm growth dynamics²⁸ or quantified diffusion limitations through the biofilm.²⁹ In a typical flow cell study, a confluent bacteria lawn is grown in a transparent chamber. These systems tend to be relatively large, with the surface area of biofilm in a typical flow cell extending over several square millimeters (e.g., ranging from 2.4 mm²³⁰ to 960 mm²).³¹ Biofilm in the chamber is typically exposed to a constant antimicrobial concentration at the biofilm–antimicrobial solution interface,³² and the response of the biofilm is observed at steady state using an inverted microscope.³³ This technique has also been used to measure diffusion of fluorescent tracers,³⁴ to quantify antimicrobial penetration velocity,²² and to characterize the microstructure of biofilms.^{10,35–37}

Microfluidic approaches are used increasingly in microbiology; for example, to study cellular responses to chemical signals³⁸ and O₂ availability.³⁹ Microfluidic approaches have employed a variety of cell culture geometries, including coculture⁴⁰ and individual cell trap⁴¹ designs. Microfluidic devices offer the advantages of controlled geometry and operating conditions with direct optical analysis at micrometer-scale resolution.⁴² Physical features and chemical gradients in microfluidic devices can match the spatial and temporal scale of real microbial habitats.⁴³ Recently, investigators have also employed microfluidics to study biofilms, including measuring the effects of shear stress,²⁶ or of divalent metal ion,²⁷ or of O₂ concentrations on the attachment of bacteria to substrates.⁴⁴ Benoit et al. used a pneumatic multiwell microfluidic design to measure single-end point responses of 24 biofilms grown in microscale flow cells.²¹ Kim et al. used a microfluidic device to study susceptibility of a continuous biofilm to a steady-state antibiotic gradient.³⁰ They grew a single confluent 300 μm (width) × 50 μm (height) × 8 mm (length) *P. aeruginosa* PAO1 biofilm in a microfluidic flow cell and then challenged different positions across the biofilm with different steady-state antimicrobial concentrations. The authors conclude that this device can be useful for screening minimal biofilm eradication concentration (MBEC) by associating responses at various positions in the biofilm with the corresponding overlying antimicrobial concentrations. A more intricate design by Kim et al. challenged eight biofilms in separate flow cells with the graduated effluent of a microfluidic mixer.⁴⁵ However, there is no existing assay to study biofilm responses to different antimicrobial dosing rates.

Dose and dosing rate information is essential in the safe and effective administration of any pharmaceutical agent. However, in the case of antibiotics, where bacterial pathogens may acquire, inherit, and spread resistance traits, optimal dosage is especially

important for maximal reduction in bacterial load and for minimizing the emergence of resistant strains.⁴⁶

In this study, a novel dynamic dosing assay is described to relate real-time respiration responses of *Staphylococcus aureus* biofilms to changing microchemical conditions. In a schematic, we illustrate how our system differs from existing techniques in terms of the time course of antimicrobial exposure. In the predominant high-throughput assay (Figure 1a), suspended

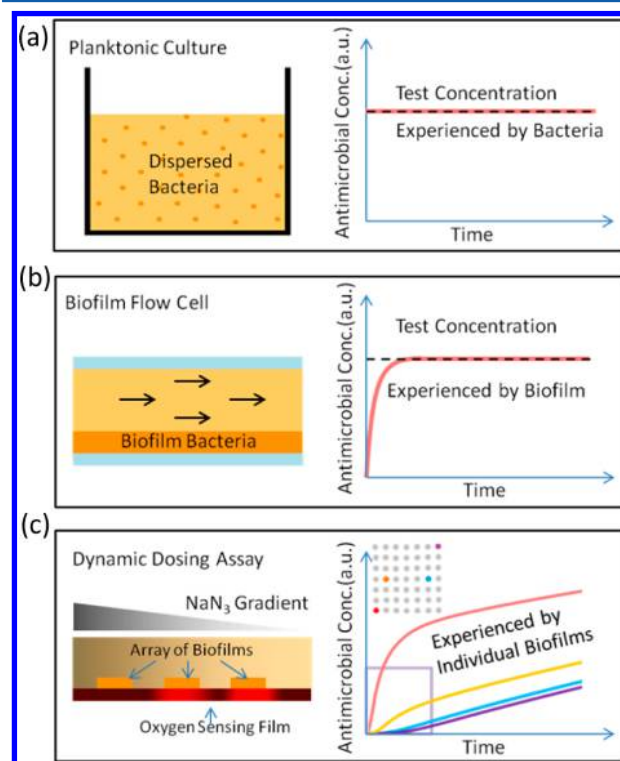


Figure 1. Typical experimental approaches used for studying antimicrobial inhibition of bacteria, and the resulting time course of antimicrobial concentration experienced by bacteria. (a) Planktonic bacteria suspended in liquid culture experience a single constant antimicrobial concentration. (b) In a typical biofilm flow cell system, a single concentration flows across a biofilm, and the response of the biofilm is monitored from below. (c) In our dynamic dosing assay, biofilms at different positions experience different and dynamically changing antimicrobial concentrations. Here, the antimicrobial is loaded on the left in the side view, and nearest the red biofilm in the 7 × 7 array inset. In the side view, fluorescence intensity under biofilms is quenched with NaN₃-induced changes in biofilm respiration. Colored lines in the graph reflect simulated concentration profiles at the corresponding positions in the array. The lower-left square indicates the time domain of the dynamic experiments described here.

bacteria are exposed to constant antimicrobial concentrations. In biofilm flow cell studies (Figure 1b), the antimicrobial diffuses into the film until the antimicrobial concentration approaches a steady-state value. In our dynamic dosing assay (Figure 1c), antimicrobial concentration varies continuously with both position and time throughout the biofilm array. The precisely controlled geometry of the microfluidic diffusion chamber causes antimicrobial concentration and flux to vary in a predictable fashion across the array. Meanwhile, respiration responses of individual biofilms are determined optically by measuring relative fluorescence of an O₂-quenched fluorophore dispersed in a thin polystyrene film.^{47,48}

To validate the dynamic dosing assay, we show sequential respiration inhibition of *S. aureus* biofilms exposed to NaN_3 . This small molecule respiration inhibitor impairs *S. aureus* catalase activity and leads to accumulation of toxic H_2O_2 .^{49,50} Local O_2 depletion under biofilms is measured in real time by measuring relative fluorescence quenching in the film. Finally, microbial responses are related to the local concentration and dosing rate of the antimicrobial.

EXPERIMENTAL SECTION

Device Concept. The dynamic dosing assay is comprised of four perimeter source wells and one central sink well. The geometry of the assay and the concentration and diffusivity of the antimicrobial determine the time-dependent diffusive flux throughout a gel-filled diffusion field containing a 7×7 biofilm array (Figure 2). A key feature of the dynamic dosing assay design

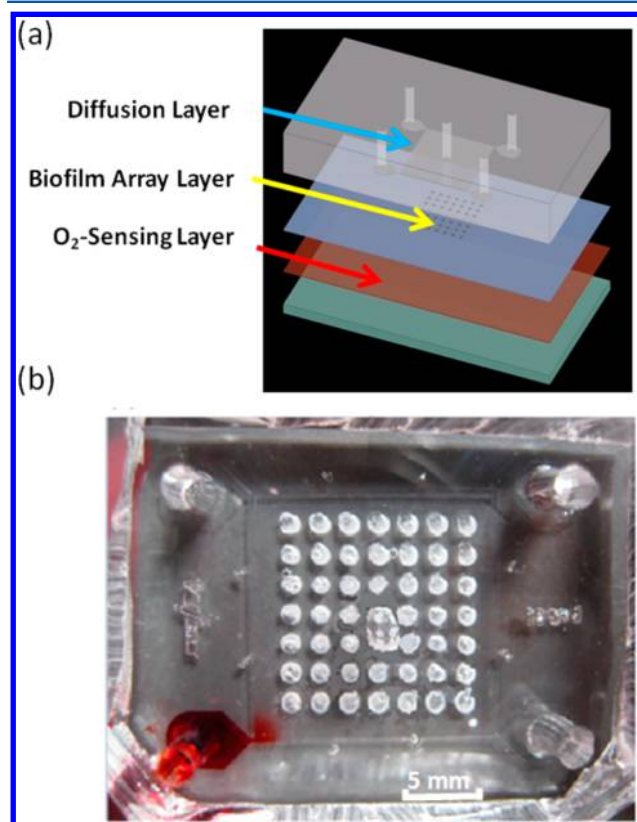


Figure 2. Schematic of the dynamic dosing assay. (a) The dynamic dosing assay consists of an O_2 -sensing film on a glass slide, a PDMS layer with a biofilm array patterned on top, all overlain by a PDMS microfluidic diffusion chamber. (b) Photograph of a biofilm array enclosed in a dynamic dosing assay, with red dye loaded in the lower-left perimeter source well.

is that the antimicrobial can be delivered to different positions at different dosing rates. Also, up to four different solutes can be loaded into the corner wells, leading to a dynamically changing antimicrobial mixture across the diffusion field. Here, we introduce an antimicrobial in only one well, so due to symmetry, we achieve 21 duplicated conditions plus the diagonal elements, for a total of 27 distinct and dynamic microchemical environments.

Device Fabrication. The microfluidic diffusion chamber of the dynamic dosing assay and the stamp for bacteria contact printing were fabricated using standard techniques of photo-

lithography and soft lithography. Briefly, $210 \pm 20 \mu\text{m}$ (Dektak model 150, Veeco Instruments, Plainview, NY) SU-8 2100 (Microchem, Newton, MA) was spin-coated onto a 3 in. diameter Si wafer (Nova Electronic Materials, test grade, Flower Mound, TX) and patterned using UV light ($45 \text{ mW}/\text{cm}^2$, 11 s, Suss Microtec, model MA6/BA6, Germany) with a chrome-on-glass photolithography mask (Advanced Reproductions, North Andover, MA).

Microfluidic devices were cast in polydimethylsiloxane (PDMS, Sylgard 184, Dow Corning, Midland, MI) mixed in a 10:1 ratio with curing agent and degassed in a vacuum desiccator at -75 kPa gage for 15 min. Degassed PDMS poured over the master was cured at $60 \text{ }^\circ\text{C}$ for 2 h. In all experiments, the height of the PDMS was $8 \pm 0.5 \text{ mm}$. Wells were punched with a 3 mm diameter biopsy punch (Miltex, Inc., York, PA).

We also used epoxy masters cast from PDMS devices in some experiments. Epoxy and epoxy curing agent (Environmental Technology, Inc., Fields Landing, CA) were mixed in a 1:1 ratio and then degassed for 20 min. A PDMS device was then placed feature-side-down into the epoxy, taking care to allow trapped air to escape, and cured in a level chamber for 2 days at room temperature.

O_2 -Sensing Film Fabrication. The available O_2 concentration under individual biofilms was determined from the relative fluorescence intensity of Pt (II) meso tetra-(pentafluorophenyl) porphyrin (Frontier Scientific Inc., Logan, UT) with O_2 quenching. Pt porphyrin has been used in previous studies for imaging O_2 gradient⁵¹ and bacteria respiration.^{52,53} Fluorescence quenching of Pt (II) meso tetra-(pentafluorophenyl) porphyrin with O_2 is reversible and fast,⁴⁷ making it an effective real-time indicator of local O_2 concentration.

Here, polystyrene films of dispersed Pt porphyrin were cast on glass microscope slides ($70 \text{ mm} \times 127 \text{ mm}$, 1 mm thick, Ted Pella, Inc., Redding, CA) precleaned with ethanol. Three solutions were spin-coated on each glass slide consecutively. For the first solution, 1 g of polyvinyl alcohol (Sigma-Aldrich, St. Louis, MO) was dissolved in 100 mL of DI water and 11.5 mL of this solution was spread on the glass slides by spinning at 4000 rpm for 40 s. For the second solution, 10 g of polystyrene beads (Mallinckrodt Baker, Inc., Phillipsburg, NJ; ACS reagent grade), and then 0.1 g of Pt (II) meso tetra-(pentafluorophenyl) porphyrin (Frontier Scientific, Inc., Logan, UT) was added, and 11.5 mL of this solution was spin-coated on the polyvinyl-alcohol layer at 4000 rpm for 40 s. Finally, PDMS premixed in 10:1 ratio with a curing agent was thinned with hexane (Certified ACS, Fisher Scientific, Fair Lawn, NJ) at proportions of 2 g PDMS to 1 mL hexane. The mixture was degassed for 5 min, and 16 mL were coated on the slide as follows: ramp to 500 rpm in 5 s, hold 13 s, then accelerate to 2700 rpm in 7 s and hold 1 min. Coated slides were cured at $60 \text{ }^\circ\text{C}$ for 2 h and then stored in the dark at room temperature. The thickness of the PDMS layer was $12.1 \mu\text{m} \pm 0.6 \mu\text{m}$.

Patterning Biofilm Array. Next, we used contact printing to produce a biofilm array of *S. aureus*. *S. aureus* is commonly used as a model for biofilm-associated opportunistic human pathogens. Contact printing methods have been evaluated in previous studies.^{54–56} Specifically, Xu et al. have shown that this method does not change the physiological state of the transferred cells.⁵⁴

Here, *S. aureus* (ATCC 25904) was incubated overnight in Tryptic Soy Broth (TSB) at $37 \text{ }^\circ\text{C}$. Stationary cultures were adjusted to $\text{OD}_{600} 1.1$ with fresh TSB media, and then $400 \mu\text{L}$ was transferred to a Tryptic Soy Agar (TSA) plate and spread

with a sterilized loop. The plate was incubated at 37 °C for 9 h in humid air. This procedure results in a continuous homogeneous bacteria lawn that was used as the “ink pad” in the subsequent stamping step.

Next, our custom PDMS stamp was pressed gently into the bacteria lawn, and then immediately placed on the prepared substrate (Figure S-1 of the Supporting Information). Our prepared substrate was an O₂-sensing film (coated slide) that had been previously plasma-treated for 45 s in an evacuated air atmosphere (Harrick PDC-32G, Harrick Plasma, Ithaca, NY). Biofilm heights of six biofilms from six separate stampings of two bacterial lawns were measured using confocal microscopy and averaged 51 ± 23 μm (mean ± std deviation).

We note that the term “biofilm” has been used to describe bacterial colonies grown on an agar plate.¹⁰ Although their structure may differ from other biofilm forms, such as flow cell biofilms grown under shear stress, the high cell density, active respiration, and lack of bulk mixing in our array results in O₂ and other gradients and imparts phenotypic differentiation with depth.

After stamping, the featured side of the PDMS diffusion chamber was plasma-treated for 45 s and bonded to the substrate with the biofilm dots aligned in the observation field. The chamber was filled with 37 °C 8% gelatin type B (ACROS, Morris Plains, NJ) dissolved in TSB solution delivered near simultaneously to all four perimeter source wells. Gelatin solution in the reservoirs was removed before gelation, while the observation field remained full due to the high surface tension of water and the small dimensions of the connecting channels. Filling the microfluidic diffusion chamber with hydrogel eliminates pressure-driven flow which, if present, would dominate diffusion. In our experiments, four such microfluidic diffusion chambers were bonded to a single O₂-sensing substrate each time experiments were performed. Three were used for replicate antimicrobial treatments or control experiments and contained bacterial biofilm arrays. The fourth chamber contained no bacteria and served as a background control for relative fluorescence of the O₂-sensing film. All four dynamic dosing assays were surrounded by a water reservoir to prevent drying.

Dynamic Respiration Inhibition Experiments. After gelation in the diffusion field, liquid aqueous NaN₃ (Laboratory grade, Fisher Scientific, Fair Lawn, NJ) was added to one source well of each microfluidic diffusion chamber while sterilized DI water was loaded in the center sink well. The other three source wells contained only air. Finally, a layer of clear tape was placed across the top of each microfluidic diffusion chamber to prevent evaporation and to prevent debris from falling into source or sink wells. The concentration gradient between the NaN₃-filled perimeter source well and the central sink well provided the driving force for diffusion. In replicate experiments, we added 3100 mM or 6100 mM NaN₃ to the source well. The steep gradient between the source well concentration and the changing diffusion field concentration ensured that a high antimicrobial flux was sustained. This high flux effectively shortens the time required to reach inhibitory concentrations throughout the biofilm array. These gradients are reproducible, as indicated by images of dye diffusion with time in replicated devices (Figure S-2 of the Supporting Information).

Constant-Concentration Respiration Inhibition Experiments. As an aid to interpreting the dynamic respiration inhibition experiments, constant-concentration respiration inhibition experiments were also performed. Here, biofilm arrays identical to those used in the dynamic experiments were

embedded in gelatin hydrogels initially containing 0 mM, 0.03 mM, 0.1 mM, and 1 mM NaN₃. Trends among specific fluorescence (area-averaged net fluorescence intensity/area-averaged net opacity) were determined to identify the steady-state concentration of NaN₃ that inhibits respiration of biofilms.

Biofilm Imaging and Analysis. Real-time fluorescence images of the O₂-sensing film under each biofilm in the array were recorded and analyzed to determine local O₂ availability as the respiration inhibitor diffused through the assay.

Fluorescence images were captured using a Carl Zeiss AXIO-observer Z1 automated inverted microscope equipped with an AxioCam MRmRev.3 camera (Carl Zeiss Inc., Germany) using a 5× objective (Zeiss ECPlan-NEOFLUAR; 5 × /0,16 ∞/0,17, Carl Zeiss Inc.). A custom-designed dichroic filter set was used to excite the film at 380 nm and measure emission at 647 nm. The set contains an excitation filter (380/14 BrightLine Bandpass Filter, FF01-380/14-25, Carl Zeiss Inc.), a Dichroic Beamsplitter (520 nm BrightLine Dichroic Beamsplitter, FF520-Di02-25 × 36, Carl Zeiss Inc., Germany) and an emission filter (647/57 BrightLine Bandpass Filter, FF01-647/57-25, Carl Zeiss Inc., Germany). Fluorescence images of all 49 biofilms in the array and at least four positions in a gel-filled control chamber without bacteria were collected every 10 min for 1.5 h to establish baseline fluorescence intensity of each biofilm prior to antimicrobial exposure. Then, after the antimicrobial at the desired concentration was loaded into the source well, fluorescence images of each biofilm in the array and all control positions were collected every 10 min for 45 h. Computer-controlled shutters exposed each position for only 800 ms, as each image was collected. Use of a narrow-band LED light source (Carl Zeiss Inc., Germany) further limited photobleaching. Bright field images of each biofilm in the array and background control positions were also collected just prior to and 45 h after adding the antimicrobial agent. Real-time area-averaged net fluorescence intensity, I_i , of each biofilm at each time point was determined using open-source Fiji (based on ImageJ) and is defined by area-averaged intensity with mean intensity of background control positions subtracted, as indicated by

$$I_i = \frac{\int_{\text{Area}} I(x, y)_i \, dA}{A} - \bar{I}_{\text{background},i} \quad (1)$$

where $I(x, y)_i$ is the intensity matrix measured for each biofilm at time i , A is the biofilm area, and $\bar{I}_{\text{background},i}$ is the mean area-averaged intensity of similarly sized background control positions at time i . The spatial extent of biofilms was defined manually for each biofilm from the corresponding initial bright field image (Figure S-3 of the Supporting Information).

In this study, all statistical analyses were performed using Stata, version 11.2.

Mass Transport Simulations. Antimicrobial concentrations and dosing rates with position and time were simulated using COMSOL Multiphysics 4.1a. The two-dimensional plan geometry of the dynamic dosing assay was defined in AutoCAD and imported into COMSOL. Microfluidic features were extruded to 210 μm, and the source and sink wells were extruded to 8 mm. Wells were modeled using standard water properties and microfluidic regions were modeled using hydrogel properties. The three empty source wells that contained only air were modeled as no-flux boundaries. The assumptions of the model are mass transport by Fickian diffusion, no convection, with constant isotropic NaN₃ diffusivity; initial concentration $C_0 = 3100$ (0.2 g/mL) or 6100 mM (0.4 g/mL) homogeneously in

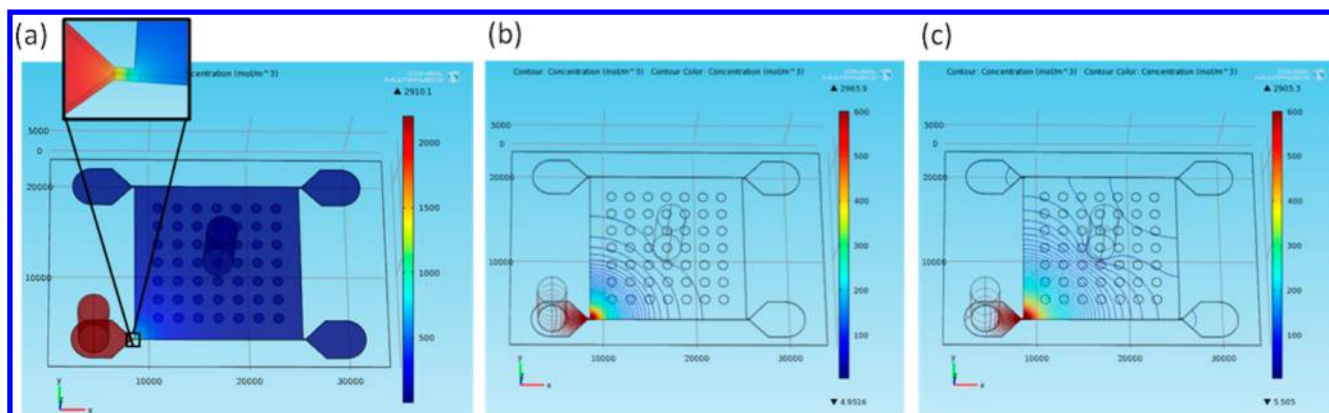


Figure 3. Simulation of NaN_3 diffusion in the dynamic dosing assay using COMSOL Multiphysics 4.1a. (a) Computer model of the microfluidic diffusion layer geometry showing 49 biofilms in the diffusion field. The tall cylinder at the lower left corner is the perimeter source that contains the antimicrobial. The center sink is the tall cylinder in the center. Simulated color-coded concentration maps are provided showing lines of constant concentration at (b) $t = 8.3$ and (c) $t = 27.7$ h.

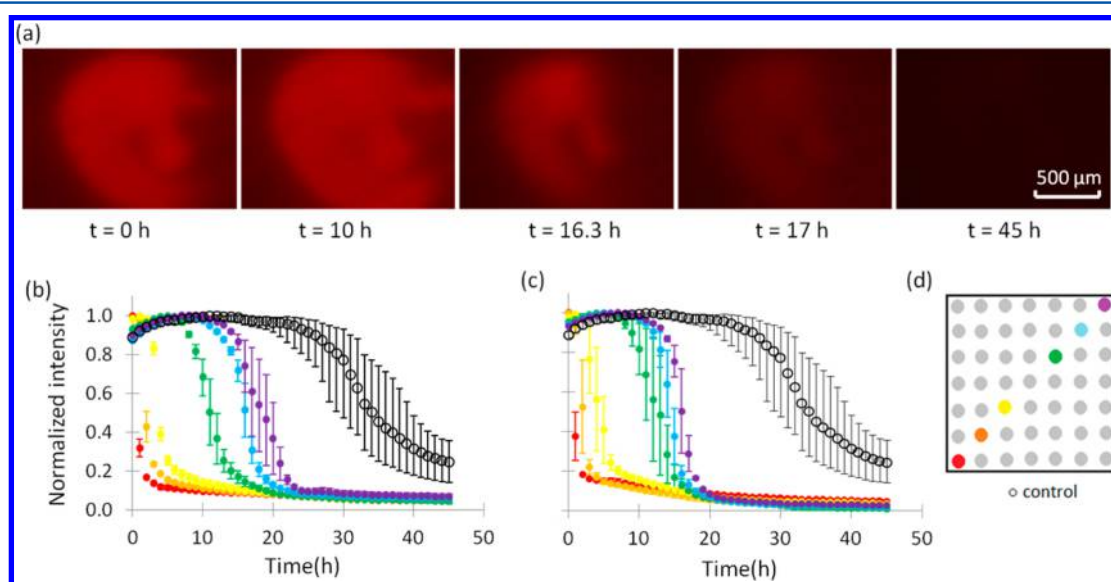


Figure 4. Real-time respiratory responses of individual biofilms with exposure of NaN_3 . (a) A representative time series of fluorescence images showing a decrease in fluorescence intensity with NaN_3 exposure. Images correspond to the blue curve in (b). (b and c) Colored markers: relative fluorescence intensities for six biofilms along a transect. Normalized intensity is area-averaged fluorescence intensity (see eq 1) normalized to maximum intensity observed for that biofilm. The source well loaded with (b) 3100 mM and (c) 6100 mM NaN_3 at $t = 0$. Data show average and range of replicate measurements in separate dynamic dosing assay devices. Open black marks: (control data) average of seven replicate biofilms exposed to 0 mM NaN_3 . The error bars show the range of replicate measurements. (See Figure S-5 of the Supporting Information for data and position of control data). (d) Schematic of biofilm array showing color coding of positions along the transect; the source well is closest to the red dot in the lower left corner.

the source well at $t = 0$, and $C_0 = 0$ elsewhere in the assay at $t = 0$; all water or gel interfaces with PDMS or air were modeled as no-flux boundaries. An array of 7×7 biofilms was defined as hydrogel cylinders with a 1 mm diameter and $50 \mu\text{m}$ height and a spatial distribution equal to the stamp and centered in the diffusion field. We assume NaN_3 solubility in water equals solubility in hydrogel, and there is no NaN_3 reaction, consumption, or volatilization.

The diffusive permeability of NaN_3 in water at 25°C has been approximated as $8.17 \times 10^{-10} \text{ m}^2/\text{s}$, as described.⁵⁷ The effective diffusive permeability of small ions through biofilm is reported to be 58% of the diffusivity in the aqueous solution⁵⁸ or $4.74 \times 10^{-10} \text{ m}^2/\text{s}$. On the basis of a previous study of diffusion in the gelatin hydrogel,⁵⁹ we defined the diffusivity of NaN_3 through 8% gelatin as $6.5 \times 10^{-10} \text{ m}^2/\text{s}$. With known initial concentrations and the defined geometry, NaN_3 concentrations and fluxes at each

biofilm position at each onset of respiration inhibition time were computed (Figure 3).

RESULTS AND DISCUSSION

Constant-Concentration Respiration Inhibition. As an independent check of the dynamic inhibition results, area-averaged net fluorescence and bright field intensities of individual biofilms and control positions were measured after exposure to fixed NaN_3 concentrations. The area-averaged bright field intensity of biofilm i is subtracted from averaged bright field intensity of the background control positions. The magnitude of the difference was defined as the area-averaged opacity of each biofilm, as indicated by

$$\text{Opacity}_i = I_{\text{bf},i} - I_{\text{bf},\text{background}} \quad (2)$$

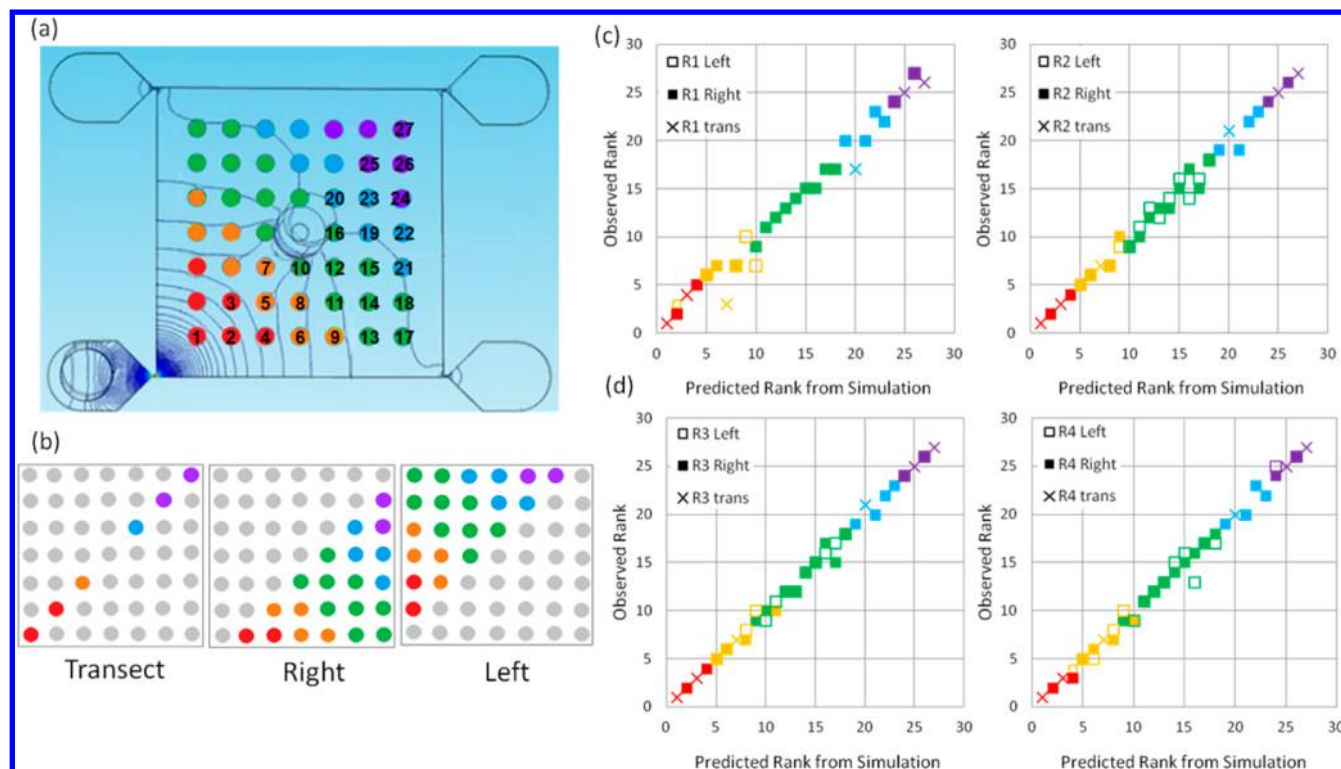


Figure 5. Ordering of the observed onset of respiration times for individual biofilms versus the predicted ranking based on the diffusion simulation. (a) Schematic of biofilm array showing predicted ranking from 1 to 27 based on diffusion simulation for positions in the array. Inhibitor is placed in the source well nearest position 1. Biofilms are organized into five groups based on proximity to the source well: Red group (positions 1–4), Orange group (positions 5–9); Green group (positions 10–18), Blue group (positions 19–23), and Purple group (positions 24–27) are shown. Contours represent constant flux at $t = 27.7$ h. (b) Schematic showing diagonal symmetry of 27 elements, for a total of 48 positions. The biofilm beneath the sink well was excluded. (c) Replicates with 3100 mM in the source well. (d) Replicates with 6100 mM in the source well. Data are plotted using different markers for the left half of the array (\square), the right half of the array (\blacksquare), and for diagonal elements (\times). Color coding of the data symbols shows the locations of each biofilm in the array.

Opacities of biofilms are assumed to be proportional to biofilm biomass, which varied in these experiments. Area-averaged net fluorescence intensities of individual biofilms following NaN_3 exposure were plotted against the corresponding opacities of the biofilms as a measure of biomass-normalized O_2 depletion as a function of NaN_3 -induced respiration inhibition (Figure S-4 of the Supporting Information). For each antimicrobial concentration, biofilms with more biomass had greater opacity and also greater area-averaged net fluorescence intensity. Controlling for biomass, we found no statistically significant difference in specific fluorescence intensity for biofilms exposed to 0 versus 0.03 mM NaN_3 . However, specific fluorescence is significantly quenched by higher NaN_3 concentrations of 0.1 mM ($p = 0.011$) and 1 mM ($p < 0.001$). We conclude that NaN_3 starts to affect biofilm respiration at concentrations between 0.03 and 0.1 mM.

Dynamic Respiration Inhibition. In duplicated diffusion experiments, either 6100 or 3100 mM NaN_3 solution was loaded in one source well of one of four different microfluidic diffusion chambers. We directly observed changing fluorescence intensities at the base of each biofilm in each array (Figure 4a) and quantified this intensity change as an area-averaged net fluorescence intensity, as described above. A plot of normalized area-averaged net fluorescence intensity versus time (Figure 4, panels b and c) shows the respiratory responses for biofilms located along a diagonal transect. Biofilms located closest to the NaN_3 -filled source well exhibit respiration inhibition first and biofilms located further away exhibit sequentially later respiration inhibition. Experiments were performed with two different NaN_3

concentrations loaded into the source wells. As expected, when a higher concentration is loaded into the source well, the driving force for diffusion is greater, and the elapsed time before respiration inhibition is observed is correspondingly shorter.

Onset of Respiration Inhibition Time. Changes in fluorescence intensity at the base of each biofilm reflect the change in available O_2 , due to changes in biofilm respiration. Healthy and actively respiring biofilms consume O_2 faster than it can be replenished by diffusion from the surroundings. Conversely, locations where biofilm respiration is inhibited by NaN_3 can experience a local increase in O_2 concentration (and therefore a quenching of fluorescence in the film). The normalized time course of fluorescence intensity at the base of the biofilm provides a measure of the changing respiration status of individual biofilms.

Although many applications will be interested in the complete time course of radial O_2 profiles, for simplicity and proof of principle, we focus on area-averaged net fluorescence intensity at one point in time for each biofilm. We define the onset of respiration inhibition (O.R.I.) time as the first of eight consecutive area-averaged net fluorescence intensity observations lower than the moving average of the four prior observations. O.R.I. time is a key moment because prior to the O.R.I. time, antimicrobial exposure is sufficiently low, such that O_2 is consumed faster than it can be replenished by diffusion. In other words, respiration is limited by the biofilm's own utilization of O_2 . After the O.R.I. time, O_2 concentration at the biofilm base begins to increase, indicating O_2 is being replenished faster than

it is consumed, and O_2 is no longer limiting. We determined O.R.I. times throughout replicate arrays loaded with different initial antimicrobial concentrations and related O.R.I. time to the corresponding local NaN_3 concentration determined from the three-dimensional diffusion simulation.

Intrinsic Respiration Inhibition. Eventually, biofilms not exposed to NaN_3 exhibit an intrinsic decrease in fluorescence intensity, presumably due to nutrient depletion. On Figure 4b and c, open markers show area-averaged net fluorescence intensity for 7 biofilms in a control experiment not exposed to the respiration inhibitor (Figure S-5 of the Supporting Information). In our experiments, the intrinsic O.R.I. time averaged 14 h. Mathematical modeling determined that all positions in the array reach a NaN_3 concentration greater than 0.1 mM within 9.1 h (with the lower concentration, 3100 mM, loaded in the source well). Therefore, we interpret respiration inhibition observed in our experiments as resulting from NaN_3 exposure, not from intrinsic respiration inhibition. The time before intrinsic respiration inhibition occurs is the available diagnostic time domain. For slowly diffusing substances, the available diagnostic time domain can be extended by using smaller biofilm dots and richer media in the gelatin (data not shown). For sparingly soluble compounds, a modified version of the microfluidic device geometry with shorter, wider inlet dimensions should be considered.

Diffusion-Based Respiration Inhibition Observed Across the Array. There are 21 biofilms in each array with a duplicate located across the diagonal axis of symmetry (Figure 5a). In addition, there are 6 diagonal elements with no replicate (the seventh position, located immediately under the sink well is excluded). Each replicated group (“left” or “right”), plus the diagonal elements, can be ordered from 1 to 27 based on the predicted time to reach a threshold antimicrobial concentration (predicted rank from simulation, Figure 5b). On the basis of diffusion modeling, the first position to reach the threshold antimicrobial concentration is defined as position 1, and it is located nearest the source well. The last position to reach the threshold concentration is defined as position 27, and it is located farthest from the source well. Generally, ordering in the array proceeds according to a straight-line distance between the source well and the biofilm, but there are exceptions. Positions 10, 16, and 20 are in close proximity to the central sink well, which depresses local concentrations.

For each biofilm position in each group, the time when O.R.I. was observed was ranked from 1 to 27 and defined as the observed rank. Then, this “observed rank” was plotted against the corresponding “predicted rank from simulation.” The data show that the observed order in which biofilms exhibited respiration inhibition closely tracked the predicted ordering based on the diffusion simulation for both low (Figure 5c) and high (Figure 5d) NaN_3 concentrations. Note that the predicted rank is not a function of test concentration. While antimicrobial concentration in the source well changes absolute O.R.I. time, it does not change the relative time among positions.

Onset of Respiration Inhibition Concentration. O.R.I. concentrations corresponding with measured O.R.I. times were determined for each position in each replicate dynamic respiration inhibition experiment ($n = 192$), using the diffusion simulation. The mean O.R.I. concentration for all dynamic experiments was 0.070 mM (see Figure S-6 of the Supporting Information for all data), midway through the 0.03 to 0.1 mM range determined for the constant-concentration experiments.

The inner 90% of O.R.I. values ranged from 0.012 mM to 0.12 mM, with a standard deviation of 0.033.

We determined the influence of experimental treatment (3100 or 6100 mM), biofilm area, and antimicrobial dosing rate on the O.R.I. concentrations. Experiments with 3100 mM in the source well (average O.R.I. concentration 0.073 ± 0.035 , mean \pm std deviation) were not statistically different from experiments with 6100 mM in the source well (average O.R.I. concentration 0.068 ± 0.031 , $p = 0.358$, t test, 2-tailed). This is an important result because the user of the assay will generally not know the effective inhibitory concentration, and our assay allows for consistent respiration inhibition concentration results, even when different source concentrations are used in the assay.

Biofilm surface area was measured by manually marking the outer perimeter of each biofilm bright field image as described above. The average area of our 192 test biofilms was 1.5 ± 0.26 mm² and ranged from 0.80 to 2.1 mm². (This area is slightly larger than the dimensions of the stamp because of spreading.) O.R.I. concentration was not significantly correlated with biofilm area ($\rho = 0.013$, $p = 0.862$). This result may seem counterintuitive since the volume for O_2 consumption increases faster than the surface area for mass transport in larger biofilms. However, our biofilms have a very small aspect ratio of depth compared with length or width, and a pseudo-one-dimensional geometry is suitable for all.

Finally, we evaluated the correlation between O.R.I. concentration and position in the array. Here, position is also linked to the antimicrobial dosing rate. Biofilms were grouped into five zones based on proximity to the source well (Figure 5). Zone 1 (red), where the highest antimicrobial dosing rates were observed, includes elements 1–4; zone 2 (orange) includes elements 5–9; zone 3 (green) contains elements 10–18; zone 4 (blue) contains elements 19–23; and zone 5 (purple) contains elements 24–27. O.R.I. concentration increased with increasing distance from the source well (ANOVA, $p < 0.001$); however, the variation in O.R.I. concentration with position was slight. Average O.R.I. concentration (\pm std deviation) by zone was 0.039 ± 0.036 for zone 1, 0.057 ± 0.030 for zone 2, 0.073 ± 0.024 for zone 3, 0.088 ± 0.027 for zone 4, and 0.088 ± 0.036 for zone 5. These results could be evidence of a slight dosing rate-dependence on *S. aureus* susceptibility to NaN_3 . However, no mechanism is known for dosing rate-dependent susceptibility of *S. aureus* to NaN_3 . The results could also be due to an artifact of the modeling assumptions, such as actual depletion of NaN_3 that is not captured by the model or slight flaws in the geometry of the microfluidic diffusion chamber.

CONCLUSION

Respiratory responses of an array of biofilms to different antimicrobial concentrations and dosing rates can be determined using the dynamic dosing assay described here. Incorporation of an optical O_2 sensor allows local changes in respiration to be observed in real time as a function of a changing microchemical environment. Here, we validated the assay by measuring respiration inhibition of *S. aureus* biofilms exposed to constant or dynamically changing NaN_3 concentrations. The results showed that respiration inhibition was observed for NaN_3 exposures above approximately 0.07 mM, regardless of the mode of exposure or size of the biofilms. A slight position dependence on the inhibitory concentration was observed. Measurement of actual NaN_3 concentrations throughout the array in situ would be needed to independently confirm dosing rate-related differences in biofilm susceptibility.

Unlike most commonly used methods to study biofilm susceptibility, our assay allows biofilm respiration inhibition to be observed in situ and permits many different antimicrobial concentrations and dosing rates to be studied in parallel. Dosing rate is known to influence bacterial susceptibility to antibiotics through variable expression of antibiotic cleavage enzymes⁶⁰ or efflux pumps⁶¹ (short-term effect) or lateral gene transfer (longer-term effect). The assay described and validated here could be used to understand the effects of quickly versus gradually increasing or oscillating antimicrobial concentrations on the evolution of tolerance and resistance in biofilm-associated bacterial populations.

Application of this assay for biofilm inhibition screening, using conventional antimicrobials and antimicrobial combinations, is the subject of ongoing work. Other extensions of this work include incorporation of additional spatially resolved sensors of microbial activity, such as optical tracking of short-lifetime fluorescent proteins expressed by the bacteria. The method described here may accelerate the study of biofilm susceptibility to individual or combinatorial therapies and may contribute mechanistic understanding of emerging biofilm resistance.

■ ASSOCIATED CONTENT

● Supporting Information

Additional information as noted in text. This material is available free of charge via the Internet at <http://pubs.acs.org>.

■ AUTHOR INFORMATION

Corresponding Author

*E-mail: leslie.shor@uconn.edu.

Notes

The authors declare no competing financial interest.

■ ACKNOWLEDGMENTS

The authors gratefully acknowledge financial support from the University of Connecticut, NSF award 0649883, USDA AFRI 2012-67020-19380, the U.S. Defense Threat Reduction Agency Grant HDTRA-09-1-0013, and support from the Vanderbilt Institute for Integrative Biosystems Research and Education (VIIBRE) and its undergraduate research program funded by Gideon Searle, the Systems Biology and Bioengineering Undergraduate Research Experience (SyBBURE). The authors thank Dr. Daniel Gage, Dr. Jessica Chau, Mr. Reed Goodwin, and Dr. Marcy Balunas for helpful discussions. We gratefully acknowledge Mr. Grant M. Bouchillon for help with computer drawing, modeling, and fabrication, Mr. David K. Schaffer for technical support in microfabrication, Ms. Vanessa Allwardt for microbiological methods development, Ms. Allison Price for editorial assistance, as well as two anonymous reviewers for many helpful suggestions.

■ REFERENCES

- (1) Stewart, P. S.; Franklin, M. J. *Nat. Rev. Microbiol.* **2008**, *6*, 199.
- (2) Anderson, G.; O'Toole, G. *Curr. Top. Microbiol. Immunol.* **2008**, *322*, 85.
- (3) Herzberg, M.; Elimelech, M. *J. Membr. Sci.* **2007**, *295*, 11.
- (4) Rao, T. S.; Kora, A. J.; Chandramohan, P.; Panigrahi, B. S.; Narasimhan, S. V. *Biofouling* **2009**, *25*, 581.
- (5) Matz, C.; McDougald, D.; Moreno, A. M.; Yung, P. Y.; Yildiz, F. H.; Kjelleberg, S. *Proc. Natl. Acad. Sci. U.S.A.* **2005**, *102*, 16819.
- (6) Weller, D. M. *Annu. Rev. Phytopathol.* **1988**, *26*, 379.
- (7) Or, D.; Phutane, S.; Dechesne, A. *Vadose Zone Journal* **2007**, *6*, 298.

- (8) Nishimura, S.; Tsurumoto, T.; Yonekura, A.; Adachi, K.; Shindo, H. *J. Orthop. Sci.* **2006**, *11*, 46.
- (9) Surdeau, N.; Laurent-Maquin, D.; Bouthors, S.; Gelle, M. P. *Journal of Hospital Infection* **2006**, *62*, 487.
- (10) Anderl, J. N.; Franklin, M. J.; Stewart, P. S. *Antimicrob. Agents Chemother.* **2000**, *44*, 1818.
- (11) Brazier, J. S.; Raybould, R.; Patel, B.; Duckworth, G.; Pearson, A.; Charlett, A.; Duerden, B. I.; Network, H. P. A. R. M. *Eurosurveillance* **2008**, *13*, 541–544.
- (12) Perez, F.; Salata, R.; Bonomo, R. *Infect. Drug Resist.* **2008**, *27*.
- (13) Pereira, S. G.; Paixao, J.; Leitao, R.; Cardoso, O. *Lett. Appl. Microbiol.* **2011**, *53*, 518.
- (14) Nelson, L. K.; Stanton, M. M.; Elphinstone, R. E. A.; Helwerda, J.; Turner, R. J.; Ceri, H. *Microbiology* **2010**, *156*, 3699.
- (15) Pagedar, A.; Singh, J.; Batish, V. K. *J. Dairy Res.* **2012**, *79*, 383.
- (16) Presterl, E.; Hajdu, S.; Lassnig, A. M.; Hirschl, A. M.; Holinka, J.; Graninger, W. *Antimicrob. Agents Chemother.* **2009**, *53*, 3205.
- (17) Houari, A.; Di Martino, P. *Lett. Appl. Microbiol.* **2007**, *45*, 652.
- (18) Muesken, M.; Di Fiore, S.; Romling, U.; Haeussler, S. *Nat. Protoc.* **2010**, *5*, 1460.
- (19) Curtin, J.; Cormican, M.; Fleming, G.; Keelehan, J.; Colleran, E. *Antimicrob. Agents Chemother.* **2003**, *47*, 3145.
- (20) Ceri, H.; Olson, M. E.; Stremick, C.; Read, R. R.; Morck, D.; Buret, A. *J. Clin. Microbiol.* **1999**, *37*, 1771.
- (21) Benoit, M. R.; Conant, C. G.; Ionescu-Zanetti, C.; Schwartz, M.; Matin, A. *Appl. Environ. Microbiol.* **2010**, *76*, 4136.
- (22) Takenaka, S.; Trivedi, H. M.; Corbin, A.; Pitts, B.; Stewart, P. S. *Appl. Environ. Microbiol.* **2008**, *74*, 1869.
- (23) Meyer, M. T.; Roy, V.; Bentley, W. E.; Ghodssi, R. *J. Microeng. Microfab.* **2011**, *21*.
- (24) Zhang, W.; Sileika, T. S.; Chen, C.; Liu, Y.; Lee, J.; Packman, A. I. *Biotechnol. Bioeng.* **2011**, *108*, 2571.
- (25) Rusconi, R.; Lecuyer, S.; Guglielmini, L.; Stone, H. A. *J. R. Soc., Interface* **2010**, *7*, 1293.
- (26) Park, A.; Jeong, H.-H.; Lee, J.; Kim, K. P.; Lee, C.-S. *BioChip J.* **2011**, *5*, 236.
- (27) Shumi, W.; Lim, J.; Nam, S.-W.; Lee, K.; Kim, S. H.; Kim, M.-H.; Cho, K.-S.; Park, S. *BioChip J.* **2010**, *4*, 257.
- (28) Lee, J.-H.; Kaplan, J. B.; Lee, W. Y. *Biomed. Microdevices* **2008**, *10*, 489.
- (29) Waharte, F.; Steenkeste, K.; Briand, R.; Fontaine-Aupart, M.-P. *Appl. Environ. Microbiol.* **2010**, *76*, 5860.
- (30) Kim, K. P.; Kim, Y.-G.; Choi, C.-H.; Kim, H.-E.; Lee, S.-H.; Chang, W.-S.; Lee, C.-S. *Lab Chip* **2010**, *10*, 3296.
- (31) Olson, M. E.; Slater, S. R.; Rupp, M. E.; Fey, P. D. *J. Antimicrob. Chemother.* **2010**, *65*, 2164.
- (32) Macia, M. D.; Perez, J. L.; Molin, S.; Oliver, A. *Antimicrob. Agents Chemother.* **2011**, *55*, 5230.
- (33) Merritt, J. H.; Kadouri, D. E.; O'Toole, G. A. *Current Protocols in Microbiology*; Wiley: Hoboken, NJ, 2005; pp 1B.1.1–1B.1.18.
- (34) Stewart, P. S.; Davison, W. M.; Steenbergen, J. N. *Antimicrob. Agents Chemother.* **2009**, *53*, 3505.
- (35) Hentzer, M.; Teitzel, G. M.; Balzer, G. J.; Heydorn, A.; Molin, S.; Givskov, M.; Parsek, M. R. *J. Bacteriol.* **2001**, *183*, 5395–5401.
- (36) Sauer, K.; Camper, A. K.; Ehrlich, G. D.; Costerton, J. W.; Davies, D. G. *J. Bacteriol.* **2002**, *184*, 1140.
- (37) Davies, D. *Nat. Rev. Drug Discovery* **2003**, *2*, 114.
- (38) Park, E. S.; Brown, A. C.; DiFeo, M. A.; Barker, T. H.; Lu, H. *Lab Chip* **2010**, *10*, 571.
- (39) Lam, R. H. W.; Kim, M.-C.; Thorsen, T. *Anal. Chem.* **2009**, *81*, 5918.
- (40) Hammoudi, T. M.; Lu, H.; Temenoff, J. S. *Tissue Eng., Part C* **2010**, *16*, 1621.
- (41) Chung, K.; Rivet, C. A.; Kemp, M. L.; Lu, H. *Anal. Chem.* **2011**, *83*, 7044.
- (42) Crane, M. M.; Chung, K.; Stirman, J.; Lu, H. *Lab Chip* **2010**, *10*, 1509.
- (43) Weibel, D. B.; DiLuzio, W. R.; Whitesides, G. M. *Nat. Rev. Microbiol.* **2007**, *5*, 209.

- (44) Skolimowski, M.; Nielsen, M. W.; Emneus, J.; Molin, S.; Taboryski, R.; Sternberg, C.; Dufva, M.; Geschke, O. *Lab Chip* **2010**, *10*, 2162.
- (45) Kim, J.; Hegde, M.; Kim, S. H.; Wood, T. K.; Jayaraman, A. *Lab Chip* **2012**, *12*, 1157.
- (46) Ball, P.; Baquero, F.; Cars, O.; File, T.; Garau, J.; Klugman, K.; Low, D. E.; Rubinstein, E.; Wise, R. *J. Antimicrob. Chemother.* **2002**, *49*, 31.
- (47) Cywinski, P. J.; Moro, A. J.; Stanca, S. E.; Biskup, C.; Mohr, G. J. *Sens. Actuators, B* **2009**, *135*, 472.
- (48) Tian, Y. Q.; Shumway, B. R.; Meldrum, D. R. *Chem. Mater.* **2010**, *22*, 2069.
- (49) Snyder, M. L.; Lichstein, H. C. *J. Infect. Dis.* **1940**, *67*, 113.
- (50) Lichstein, H. C.; Soule, M. H. *J. Bacteriol.* **1944**, *47*, 221.
- (51) Grate, J. W.; Kelly, R. T.; Suter, J.; Anheier, N. C. *Lab Chip* **2012**, *12*, 4796.
- (52) Montagne, K.; Komori, K.; Yang, F.; Tatsuma, T.; Fujii, T.; Sakai, Y. *Photochem. Photobiol. Sci.* **2009**, *8*, 1529.
- (53) Strovos, T. J.; Dragavon, J. M.; Hankins, T. J.; Callis, J. B.; Burgess, L. W.; Lidstrom, M. E. *Appl. Environ. Microbiol.* **2006**, *72*, 1692.
- (54) Xu, L.; Robert, L.; Qi, O.; Taddei, F.; Chen, Y.; Lindner, A. B.; Baigl, D. *Nano Lett.* **2007**, *7*, 2068.
- (55) Weibel, D.; Lee, A.; Mayer, M.; Brady, S.; Bruzewicz, D.; Yang, J.; Diluzio, W.; Clardy, J.; Whitesides, G. *Langmuir* **2005**, *21*, 6436.
- (56) Rowan, B.; Wheeler, M. A.; Crooks, R. M. *Langmuir* **2002**, *18*, 9914.
- (57) McBrady, A. D.; Chantiwas, R.; Torgerson, A. K.; Grudpan, K.; Synovec, R. E. *Anal. Chim. Acta* **2006**, *575*, 151.
- (58) Stewart, P. S. *Biotechnol. Bioeng.* **1998**, *59*, 261.
- (59) Laitinen, H. A.; Kolthoff, I. M. *J. Am. Chem. Soc.* **1939**, *61*, 3344.
- (60) Walsh, C. *Nature* **2000**, *406*, 775.
- (61) Zakeri, B.; Wright, G. D. *Biochem. Cell Biol.* **2008**, *86*, 124.